Journal of Applied Fluid Mechanics, Vol. 11, No. 5, pp. 1185-1192, 2018.
Available online at www.jafmonline.net, ISSN 1735-3572, EISSN 1735-3645.
DOI: 10.29252/jafm.11.05.28067

Effect of Turbulent Uniform Flow past a Two-Dimensional Square Cylinder

Y. C. Li[1], C. Y. Chung [2] and F. M. Fang [3†]

[1] *Wind Engineering Research Center, Tamkang University, New Taipei City, 251, Taiwan*
[2] *Aerospace Science and Technology Research Center, National Cheng Kung University, Tainan, 711, Taiwan*
[3] *Department of Civil Engineering, National Chung Hsing University, Taichung, 402, Taiwan*

†*Corresponding Author Email: fmfang@nchu.edu.tw*

(Received May 31, 2017; accepted April 4, 2018)

ABSTRACT

Turbulent uniform flows past a two-dimensional square cylinder are investigated numerically. By varying the turbulence intensity and turbulence length scale of the approaching flow, the flow effect of the cylinder are compared to that in a laminar approaching-flow case. In addition, the variations of drag and lift coefficients with respect to the changes of turbulence intensity and turbulence length scale are analyzed on a systematic basis. In the large eddy simulations, the approaching-flow turbulence is generated by a spectral method according to Kármán spectrum. Two levels of turbulence intensities (5% and 10%) and three turbulence length scales (0.25, 0.50 and 1.0 times of the cylinder width) are selected in the study to examine the effect on the cylinder. Results show that the Strouhal number remains almost unchanged when the uniform approaching-flow changes from a laminar state to a turbulent one. The approaching-flow turbulence has noticeable effect in promoting the resulting drag and lift fluctuations. However, its effect on the mean drag appears negligible. In contrast, an increase of the approaching-flow turbulence length scale leads to mild increases of the mean and root-mean-square values of drag. On the other hand, the resulting lift fluctuation is insensitive to the change of the turbulence length scale.

Keywords: Turbulent approaching flow; Square cylinder; Large eddy simulation.

NOMENCLATURE

$\bar{C}_D$	mean drag coefficient
C'_D	fluctuating drag coefficient
C'_L	fluctuating lift coefficient
C_s	proportionality coefficient
D	width of square cylinder
E_i	velocity spectra
f	frequency
F_D	drag force
F_L	lift force
f_s	shedding frequency
$I_{u,v,w}$	turbulence intensity of *u, v, w*
k	bulk modulus of elasticity
$\tilde{k}$	turbulence kinetic energy
k_0	initial wave number of generation
$k^{m,n}$	turbulence kinetic energy matrix
L_s	scaling factor, $\theta_1\sqrt{L_u^2+L_v^2+L_w^2}$
L_u	turbulence length scale
m	frequency segment
n	Fourier serious numbe
p	spaced-averaged pressure
Re	Reynolds number
$r_i^{m,n}$	three-dimensional normal distributed Random number
S_{ij}	strain tensor
St	Strouhal number
$S_{u,v,w}$	spectrum in *x, y, z* direction
t	time
U_0	mean velocity of inflow
$\vec{V}$	spaced-averaged velocity
$\tilde{x}$	dimensionless coordinate
Δ	filter width
ν	kinematic viscosity
ν_t	turbulent viscosity
θ_1	spatial correlation parameter
θ_2	time correlation parameter
ρ	density
τ_0	time normalized factor, $\theta_2 L_s / \bar{U}$
$\omega_{m,n}$	angular frequency

1. INTRODUCTION

A uniform flow past a two-dimensional square or rectangular cylinder is a typical bluff-body-flow problem, which involves fundamental researches of the surrounding flow behavior and the effect of the body. Physically, when a flow passes the body, separation is initiated at the leading edges of the cylinder due to a sudden pressure drop. The separation lines from both sides of the body roll and form pairs of alternative vortices downstream. As a result, vortex shedding phenomenon can be found in the wake region of the flow. Due to the unsteady behavior of the wake flow, therefore, the resulting drag and lift associated with the cylinder become time-dependent.

2. RELATED STUDIES

In the past, a majority of the related studies concentrated on such a flow problem under the condition that the uniform approaching flow is laminar. Measurements of the flow behavior and flow effect on the cylinder can be performed by conducting laboratory experiments. Certain typical works (Vickery 1966; Bearman and Truman 1972; Lee 1975; Pocha 1971) investigated drag, lift, surface pressure as well as shedding phenomena of separated shear flows around two-dimensional square or rectangular cylinders. On the other hand, typical numerical simulations of flows around square/rectangular bodies with a smooth approaching flow were performed by researchers using k-ε turbulence modeling (Mathews 1987; Murakami and Mochida 1988; Basara and Younis 1992) and large eddy simulations (Hanson *et al*. 1984; Han 1988). Particularly, by comparing with the measurement results of flows around a cube, Murakami *et al*. (1990) found that the adoption of large eddy simulation could provide more accurate results than using k-ε model in predicting the unsteady shear flows.

There were also a number of experimental studies regarding turbulent uniform flows past rectangular or square cylinders. Typically, Vickery (1966) found that the approaching-flow turbulence could promote the extent of pressure fluctuations on the windward and leeward surfaces of the cylinder. Hussain and Reynolds (1970) measured the behavior of wave disturbance in turbulent channel flows, which were artificially generated by using controlled vibrating ribbons. In the wind tunnel experiments by Lee (1975), Huot *et al*. (1986) and Lu *et al*. (2003), it was found that the approaching-flow turbulence could lead to an expansion of the downstream wake region. Based on the experimental results, Hillier and Cherry (1981) concluded that the mean flow-field responded strongly to approaching-flow turbulence intensity but with little effect of integral scale. The results from the experiments by Nakamura and Ozono (1987) indicated that an increase of the approaching-flow turbulence intensity could result in an early occurrence of re-attachment at the sides of a flat plate with rectangular leading-edge geometry. To conduct aeroelastic stability experiments of long-span bridges, Hann *et al*. (1998) employed a technique of lateral jets blowing to the main flow. Noda and Nakayama (2003) measured the instantaneous pressure distributions on rectangular cylinders and found that the free-stream turbulence caused pressure fluctuation on the front surface as buffeting due to the impinging turbulence.

Compared to that in numerical studies, the execution of experiments of turbulent uniform flow past a two-dimensional cylinder was considered more difficult. To obtain a turbulent uniform approaching flow in a wind or water tunnel, for instance, a grid panel was commonly set at the upstream of the test section to produce inlet flow turbulence. Since the generated turbulence was highly non-equilibrium, it usually suffered from a rapid decay along the streamwise direction. Consequently, the approaching-flow turbulence characteristics were hard to control precisely. For the same reason, it was not easy to achieve a large turbulence intensity level at the test location. On the other hand, the use of numerical simulation to deal with the analysis can be another choice. If the approaching-flow turbulence characteristics can be precisely controlled, it is more convenient to perform analysis of the problem on a systematic basis compared to the execution of experiments.

3. PROBLEM DESCRIPTION

The goal of the study is to investigate numerically the flow and its effect on a two-dimensional square cylinder with uniform approaching flows containing homogeneous turbulence. By varying the turbulence intensity and the length scale, the resulting shedding frequency (f_S), drag (F_D) and lift (F_L) were analyzed to assess the approaching-flow turbulence effect on the wake flow and the force on the body.

Figure 1 illustrates the schematic of the problem. The attack angle of the approaching flow is zero. The turbulence intensity (I_u) and length scale (L_u) in the approaching flow are referred to the component in the streamwise (x) direction. Two turbulence levels (I_u= 5% and 10%) and three turbulence length scales (L_u = 0.25D, 0.50D and 1.0D) were selected in the study. The Reynolds number (Re=U_0D/ν; ν is kinematic viscosity) was selected as 10^5.

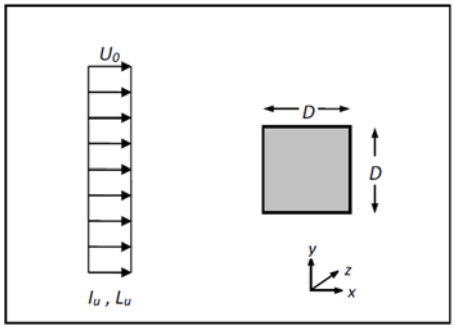

Fig. 1 Sketch of problem.

4. NUMERICAL METHOD

A weakly-compressible-flow (WCF) method (Song and Yuan 1988) was adopted in the flow simulation. In the method, the continuity and momentum equations are

$$\frac{\partial p}{\partial t} + k\nabla.\vec{V} = 0 \tag{1}$$

$$\frac{\partial \vec{V}}{\partial t} + \vec{V}.\nabla\vec{V} = -\nabla\frac{p}{\rho} + \nabla.\left[\left(\nu + \nu_t\right)\nabla\vec{V}\right] \tag{2}$$

where p and $\vec{V}$ denote respectively spaced-averaged pressure and velocity; t is time; k is the bulk modulus of elasticity of air. ν_t is the turbulent viscosity, and is determined according to a dynamic subgrid-scale turbulence model proposed by Germano *et al.* (1991). Accordingly, the turbulent viscosity is obtained as

$$\nu_t = \left(C_s\Delta\right)^2\sqrt{2S_{ij}S_{ij}};$$

$$\text{where } S_{ij} = \frac{1}{2}\left(\frac{\partial u_i}{\partial x_j} + \frac{\partial u_j}{\partial x_i}\right) \tag{3}$$

C_s , Δ and S_{ij} in Eq. (3) represent respectively the proportionality coefficient, the filter width and the strain tensor. Two filters (grid and test filters) were used to calculate C_s during the computation process. The width of the test filter was chosen as twice of that of the grid filter. To avoid numerical instability due to an extensive variation of C_s in time and space, spatial averaging in the homogeneous direction was made and interpolation was used for C_s distribution between the test (coarse) and grid (fine) filters. A three-dimensional finite-volume method with a collocated grid arrangement was used to solve the equations of motion. Second-order accuracy in space was used in the discretized equations of Eqs. 1 and 2, and Crank-Nicolson scheme was employed in time integration. The bounded central-differencing scheme was used to discretize the convection terms in the filtered momentum equation. From the pressure values at the cell centers, the face values were computed with a second-order scheme. Interpolations of values for diffusive terms from cell centers to face centers were made using a second-order central-difference scheme. The elapsed time (Δt) of the unsteady flow computations was limited by Courant-Friedrich-Lewy condition (Courant *et al.* 1967). Typically, the normalized elapsed time ($\Delta tU_0/D$) was 5×10^{-4}.

In all flow simulations, three-dimensional flow computations were carried out in a $25D\times12D\times8D$ rectangular domain and the results on the middle plane in the span-wise direction of the cylinder were taken as the basis of the analysis of the two- dimensional problem. Figure 2 depicts a typical computational mesh system ($337\times100\times80$) on the x-y plane. The smallest grid size is $0.05D$.

Appropriate values of pressures and velocities were specified at exterior cells (or phantom cells) outside the boundaries to reflect physical nature of the boundaries. At the cylinder surface, a no-slip condition was used. At the side boundaries, the pressures and velocities at the phantom cells were specified according to a zero-gradient assumption in the direction normal to the boundaries. At the inflow section, prescribed unsteady velocities were imposed and a zero-gradient condition was applied for pressure specifications. At the outflow boundary, on the other hand, a zero-gradient condition was used for the velocities, and the sectional average pressure was set as the reference pressure of the instantaneous flow field. More detail regarding the application of WCF method can be referred to the work by Chen *et al.* (Chen *et al.* 2009).

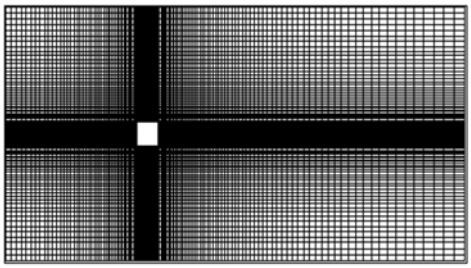

Fig. 2 Mesh system on the *x*-*y* plane.

To generate homogeneous and isotropic turbulence at the inflow section, the modified discretizing and synthesizing random flow generation (MDSRFG), proposed by Castro *et al.* (2011), was used. By prescribing given values of turbulent intensity and length scale, the generated velocity components in all the three directions (x, y and z) were obtained based on von Kármán spectrum. A brief formulation of the method is described as below.

$$U(x,t) = \sum_{m=1}^{M}\sum_{n=1}^{N}\left[p_i^{m,n}\cos\left(\tilde{k}_j^{m,n}\tilde{x}_j + \omega_{m,n}\frac{t}{\tau_0}\right) + q_i^{m,n}\sin\left(\tilde{k}_j^{m,n}\tilde{x}_j + \omega_{m,n}\frac{t}{\tau_0}\right)\right] \tag{4}$$

where

$$p_i^{m,n} = sign\left(r_i^{m,n}\right)\sqrt{\frac{4c_i}{N}E_i\left(k_m\right)\Delta k_m\frac{\left(r_i^{m,n}\right)^2}{1+\left(r_i^{m,n}\right)^2}} \tag{5}$$

$$q_i^{m,n} = sign\left(r_i^{m,n}\right)\sqrt{\frac{4c_i}{N}E_i\left(k_m\right)\Delta k_m\frac{1}{1+\left(r_i^{m,n}\right)^2}} \tag{6}$$

With $\omega_{m,n}\in N\left(0,2\pi f_m\right)$; $r_i^{m,n}$ is a three-dimensional normal distributed random number with mean value $\mu_r = 0$ and the standard deviation $\sigma_r = 1$. $c_i = 0.5\bar{U}$ and $\bar{U}$ is the mean wind speed. $\tilde{x} = x/L_s$, and $L_s = \theta_1\sqrt{L_u^2 + L_v^2 + L_w^2}$ is the scaling factor for spatial correlation. $\tau_0 = \theta_2 L_s/\bar{U}$ is the parameter

to allow for the control over the time correlation. The turbulence kinematic energy $\tilde{k}^{m,n} = k^{m,n} / k_0$ is the three-dimensional distribution on the sphere of inhomogeneous and anisotropic turbulence. The spectra E_i of three components are consistent with von Kármán models, defined as

$$S_u(f) = \frac{4\left(I_u\bar{U}\right)^2\left(L_u/\bar{U}\right)}{\left[1+70.8\left(fL_u/\bar{U}\right)^2\right]^{5/6}} \tag{7}$$

$$S_v(f) = \frac{4\left(I_v\bar{U}\right)^2\left(L_v/\bar{U}\right)\left[1+188.4\left(2fL_v/\bar{U}\right)^2\right]}{\left[1+70.8\left(2fL_v/\bar{U}\right)^2\right]^{11/6}} \tag{8}$$

$$S_w(f) = \frac{4\left(I_w\bar{U}\right)^2\left(L_w/\bar{U}\right)\left[1+188.4\left(2fL_w/\bar{U}\right)^2\right]}{\left[1+70.8\left(2fL_w/\bar{U}\right)^2\right]^{11/6}} \tag{9}$$

5. PERFORMANCE OF THE GENERATED TURBULENT APPROACHING FLOW

In each case, after the history of the generated turbulent inlet velocity at the inlet boundary corresponding to a prescribed turbulence intensity and length scale was achieved, preliminary large-eddy simulations were conducted in a computational spatial domain without the existence of the cylinder. The longitudinal variations of the resulting turbulence characteristics (turbulence intensity, turbulence scale and energy spectrum) were analyzed to examine the validity of the generated turbulence. Figure 3 illustrates a typical example (I_u=5% and L_u=0.25D) of the resulting power spectra at x=0 (inlet) and x=5D (the location where the cylinder would be set). It shows that the generated turbulence, initially meets the form of von Kármán spectrum, remains almost unchanged along the streamwise direction. Figure 4 also shows the corresponding longitudinal decay of the turbulence intensity, which reveals that the generated inlet-flow turbulence behaves well.

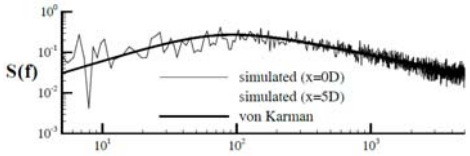

Fig. 3 Comparison of spectra of turbulence.

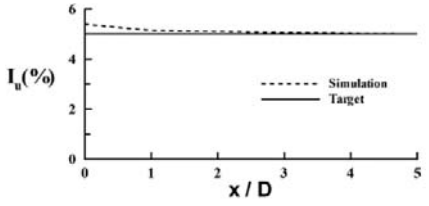

Fig 4 Longitudinal variation of turbulence intensity.

6. VERIFICATION OF THE NUMERICAL METHOD

6.1 Laminar Approaching Flow Case

To check the accuracy of the predictions by the numerical method, a flow simulation was performed in a laminar approaching-flow case (I_u = 0%) at a Reynolds number of 10^5. Table 1 illustrates the comparisons of certain selected normalized quantities between the predictions and the related results from previous experimental studies. In the table, St denotes the Strouhal number (=$f_S D/U_o$; f_s is the shedding frequency). The "bar" and "prime" denote respectively the mean and root-mean-square values; $C_D = F_D / 0.5\rho U_o^2 D$; $C_L = F_L / 0.5\rho U_o^2 D$; F_D and F_L are the drag and lift forces. Compared with the experimental results, the maximum relative differences are respectively 6.8%(St), 3.5%($\bar{C}_D$), 12.8%(C'_D) and 14.0%(C'_L). This indicates that the computational results are in fairly good agreement with those from the experiments, except some extent of discrepancies in terms of the fluctuating drag and lift coefficients.

6.2 Turbulent Approaching Flow Case

Computation of a turbulent uniform flow past a square cylinder was also conducted in a case with I_u=5.3% and L_u=1.12D at a Reynolds number of 6.89×10^4. The results of the predicted Strouhal number (St=$f_S D/U_o$) as well as the normalized coefficients of mean and root-mean-square drag and lift are listed in Table 2, together with those from the experiments by Noda and Nakayama (Noda and Nakayama 2003). The comparison shows that the fluctuating drag coefficient was over-predicted and the other quantities were predicted well.

7. RESULTS

7.1 Effect on the Strouhal Number

Based on the results of flow simulations, Fig. 5 depicts the power spectra associated with the lift of the cylinder. For all the turbulent approaching flows, it is found that the resulting Strouhal number remains almost unchanged (0.129), compared to that in the laminar approaching-flow case.

7.2 Effect on the Drag

Figure 6(a) shows the time history of the predicted drag in a typical turbulent approaching-flow case (I_u = 10% and L_u = 0.75D). Compared with that in the laminar approaching-

flow case (Fig. 6(b)), it reveals that when turbulence is contained in the approaching flow, it remains in the entire flow field and results in high-frequency components of the resulting drag force.

Figures 7 depict the predicted variations of the mean and fluctuating drag coefficients ($\bar{C}_D$ and C'_D) as functions of I_u and L_u/D. In terms of the mean drag coefficients

Table 1 Comparison of related quantities in laminar-approaching flow case.

	Re	*St*	$\bar{C}_D$	C'_D	C'_L
Calculated	10^5	0.129	2.085	0.218	1.135
Experimental (Vickery 1966)	10^5	0.12	-	-	1.32
Experimental (Bearman 1972)	$(2\sim7)\times10^5$	0.125	2.15	-	-
Experimental (Lee 1975)	1.76×10^5	0.122	2.07	-	1.23
Experimental (Pocha 1971)	9.1×10^4	0.12	2.06	0.19	-
Experimental (Lyn and Rodi 1994)	2.2×10^4	0.132	2.1		
Experimental (Noda and Nakayama 2003)	6.89×10^4	0.131	2.16	0.207	1.18

Table 2 Comparison of related quantities in a typical turbulent approaching-flow case.

	Re	I_u (%)	L_u/D	*St*	$\bar{C}_D$	C'_D	C'_L
Calculated	6.89×10^4	5.3	1.12	0.129	2.163	0.291	1.094
Experimental (Noda and Nakayama 2003)	6.89×10^4	5.3	1.12	0.133	1.989	0.203	1.105
Relative difference (%)				3.0	8.7	43.3	1.0

(see Fig. 7(a)), generally, a change of the approaching-flow turbulence level has a negligible effect on the mean drag coefficient. Meanwhile, an increase of the turbulence length scale leads to a mild increase of $\bar{C}_D$. Compared to that in the laminar approaching-flow case, for instance, the mean drag coefficient increases about 2% when L_u is equal to 1.0D.

In contrast, the root-mean-square values of the drag coefficient appear more sensitive to the approaching-flow turbulence characteristics (see Fig. 7(b)). The reason is considered to be due to the effect of turbulence originated from the inlet, and this evidence agrees with the conclusion by Noda and Nakayama (2003). Generally, a higher level of turbulence intensity promotes more significant drag fluctuations. In addition, a mildly increasing

tendency of C'_D is detected as L_u increases.

7.3 Effect on the Lift

Due to symmetry of the flow problem, the magnitude of the mean lift coefficient ($\bar{C}_L$) should be zero. Again, a typical example of lift history (I_u = 10% and L_u = 0.75D) is shown in Figs. 8, together with that in the laminar approaching-flow case. The comparison shows that the approaching-flow turbulence also has some effect on the resulting lift history. Compared to the similar tendency associated with the drag histories (Figs. 6), the effect of the lift coefficient due to the effect of approaching-flow turbulence appears relatively milder.

Based on the results of numerical computations, Fig. 9 demonstrates the variations of the fluctuating lift coefficients (C'_L) with respect to I_u and L_u. Due to the effect of approaching-flow turbulence, it is found that the extent of the fluctuating lift is also promoted, compared to that in the laminar approaching-flow case. However, the extent of the increase of lift fluctuations appears relatively less sensitive to the change of I_u. Typically, as I_u equals to 5% and 10%, the relative increases of C'_L are about 2.6% and 4.9% respectively.

8. DISCUSSION

8.1 Uncertainty Analysis of Computations

Besides that the execution of a three-dimensional unsteady turbulent numerical computation was time-consuming, the generation of approaching-flow turbulence with prescribed turbulent length scale and turbulent intensity also cost a great deal of computing time. Considering both the

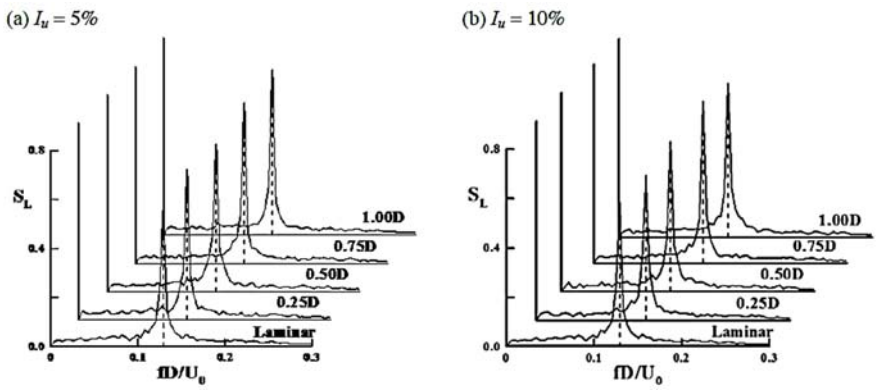

Fig. 5 Power spectra of lift.

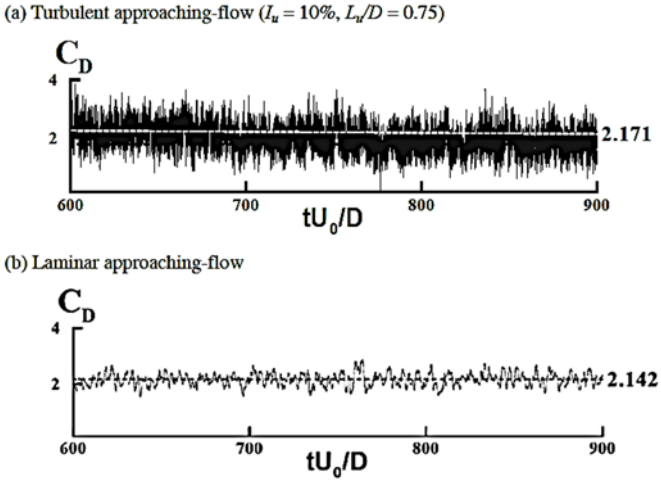

Fig. 6 Comparison of drag histories.

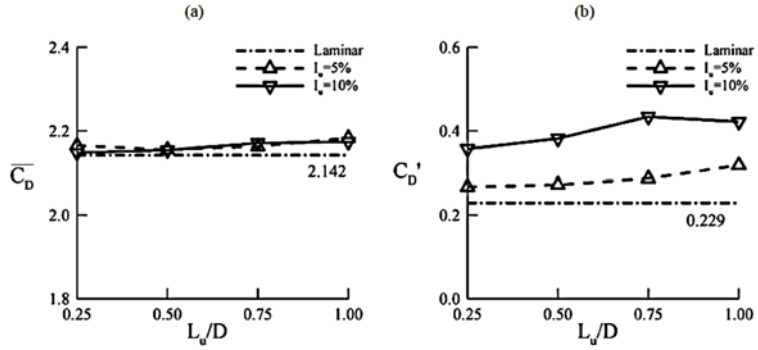

Fig. 7 Variations of drag coefficients (a) mean (b) root-mean-square

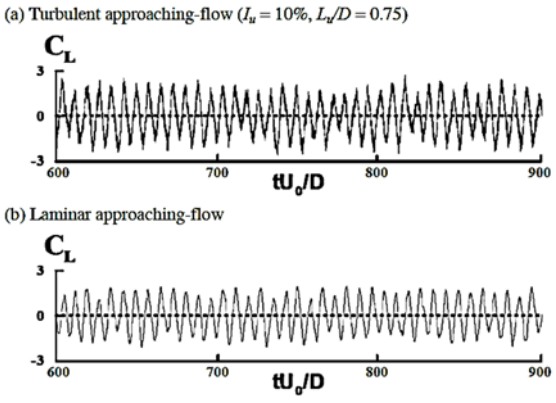

Fig. 8 Comparison of lift histories.

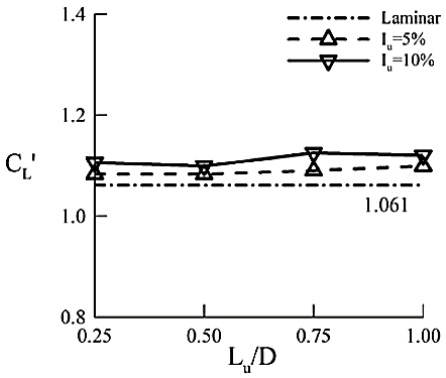

Fig. 9 Variations of root-mean-square lift coefficients.

Table 3 Typical comparison of predicted results within different statistical period (I_u = 10%, L_u/D = 0.75).

Normalized period	*Re*	I_u (%)	L_u/D	*St*	$\bar{C}_D$	C_D'	C_L'
300	10^5	10.0	0.75	0.129	2.171	0.434	1.094
600	10^5	10.0	0.75	0.130	2.167	0.431	1.090
Relative difference (%)				0.8	0.2	0.7	0.4

prediction accuracy and the time consumption of the numerical computations, the statistics of the resulting flow variables were generally performed within a normalized time period (TU_0/D; T is the real-time period) of 300. To examine the effect due to the selected length of the statistical period, additional computations were performed. Table 3 illustrates the comparison of the predicted results typically in the case that I_u and L_u/D were respectively equal to 10% and 0.75. Since the relative differences were all less than 1%, it reveals that the adoption of the statistical period is long enough to provide reliable prediction results for all the numerical computations in the study.

8.2 Longitudinal Decay of I_u

Although the prescribed approaching-flow turbulence was generated numerically based on the theoretical method by Castro *et al.* (2011), a tendency of slight longitudinal decay of the approaching-flow turbulent intensity still occurred. This should be attributed to the effect of numerical truncation error, which produces some minor non-equilibrium effect of flow turbulence. Typically, Fig. 4 indicates that the turbulent intensity at the inlet (5.4%) gradually decreased to 5% as x/D reaches about 3D. Further downstream (x/D>3), however, the state of turbulence remained well equilibrium (see also Fig. 3). This would provide a much better approaching-flow condition compared with that in experiments, which usually suffered from fast turbulence decay due to the non-equilibrium features of grid-generated turbulence.

8.3 Over-Predictions of C_D'

The comparison in Table 2 shows that the fluctuating lift coefficient (C_D') was to some extent over-predicted. As was stated, when the approaching-flow turbulence was generated by an upstream grid panel in experiments, it generally suffered from fast turbulence decay due to its highly non-equilibrium feature. That is, the turbulence level in the region near the cylinder could be lower than the prescribed one at the upstream. In contrast, the generated approaching-flow turbulence in the numerical simulation was free of longitudinal decay thus provided a better flow environment in the analysis. On the other hand, it was found that a higher level of turbulence intensity promotes more significant drag fluctuations (see Fig. 7b). This could explain why an over-prediction of C_D' was achieved. However, additional investigations would be required in the future to support this argument.

9. CONCLUSION

The flow around a two-dimensional square cylinder with turbulent uniform approaching flows was investigated numerically at a Reynolds number of 10^5. By varying the turbulence intensity and the turbulence length scale of the approaching flow, the effect on the cylinder was analyzed on a systematic basis. The results, in terms of the Strouhal number, mean and fluctuating drag coefficients and the fluctuating lift coefficient, were also compared with those in the laminar approaching-flow case. Within the test ranges of turbulence intensity and turbulence scale, several conclusions are drawn as follows:

1. As the uniform approaching flow changes from a laminar state to a turbulent one, the resulting Strouhal number remains almost unchanged.
2. When the approaching flow contains turbulence, it remains in the entire flow field and results in high-frequency components of

the drag and lift forces.

3. The approaching-flow turbulence level has almost no effect on the resulting mean drag. However, it has noticeable effect on the fluctuating drag and lift, in which the former appears more significant than the latter.

4. Although increasing tendencies of $\overline{C}_D$ and C'_D with respect to Lu are found, the extents of increase are mild. 5. The lift fluctuations are insensitive to the change of L_u.

ACKNOWLEDGEMENTS

The study was supported by the Ministry of Science and Technology in Taiwan [grant number MOST 105-2221-E-005-015].

REFERENCES

Basara, B. and Younis, B. A. (1992). Progress in the prediction of turbulent wind loading on buildings. *Journal of Wind Engineering and Industrial Aerodynamics* 41-44, 2863-2874.

Bearman, P. W. and Truman, D. M. (1972). An investigation of the flow around rectangular cylinder. *Aerodynamic Quartely* 23, 229- 237.

Castro, H. G., Paz, R. R. and Sonzogni, V. E. (2011). Generation of turbulence inlet velocity conditions for large eddy simulation. *Mecánica Computational XXX*, 2275–2288.

Chen, C. C., Fang, F. M., Li, Y. C., Huang, L. M. and Chung, C. Y. (2009). Fluid forces on a square cylinder in oscillating flows with non-zero mean velocities. *International Journal for Numerical Methods in Fluids* 60, 79-93.

Courant, R., Friedrich, K. O. and Lewy, H. (1967). On the partial differential equations of mathematical physics. *IBM Journal* 11, 215-234.

Germano, U., Piomelli, P. and Cabot, W. H. (1991). A dynamic subgrid-scale eddy viscosity model. *Physics of Fluids* 3, 1760-1765.

Haan, F. L., Kareem, A. and Szewczyk, A. A. (1998). The effects of turbulence on the pressure distribution around a rectangular prism. *Journal of Wind Engineering and Industrial Aerodynamics* 77-78, 381-382.

Han, T. (1988). Computational analysis of three-dimensional turbulent flow around a bluff body in ground proximity. *AIAA Journal* 27, 1211-1219.

Hanson, T., Summers, D. M. and Wilson, C.B. (1984). Numerical modeling of wind flow over buildings in two dimensions. *International Journal of Numerical Methods in Fluids* 4, 25-41.

Hillier, R., and Cherry, N. J. (1981). The effects of stream turbulence on separation bubbles. *Journal of Wind Engineering and Industrial Aerodynamics* 8, 49–58.

Huot, J. P., Rey, C. and Arbey, H. (1986). Experimental analysis of the pressure field induced on a square cylinder by a turbulent flow. *Journal of Fluid Mechanics*, 162:283-298.

Hussain, A. K. M. F. and Reynolds, W. C. (1970). The mechanics of an organized wave in turbulent shear flow. *Journal of Fluid Mechanics* 41, 241-258.

Lee, B. E. (1975). The effect of turbulence on surface pressure field of a square prism. *Journal of Fluid Mechanics* 69, 263-282.

Lu, P. C., Cheng, C. M., Lai, C.W. and Chang, C. W. (2003). Separated shear layers of rectangular prisms in turbulent flows. *Journal of the Chinese Institute of Engineers* 26, 721-727.

Lyn, D. and Rodi, W. (1994). The flapping shear layer formed by flow separation from the forward corner of a square cylinder. *Journal of Fluid Mechanics* 267, 353-376.

Mathews, E. H. (1987). Prediction of The wind-generated pressure distribution around buildings. *Journal of Wind Engineering and Industrial Aerodynamics* 25, 219-228.

Murakami, S. and Mochida, A. (1988). 3-D Numerical simulation of airflow around a cubic model by means of the k-ε model. *Journal of Wind Engineering and Industrial Aerodynamics* 31, 283-303.

Murakami, S., Mochida, A. and Hayashi, Y. (1990). Examining the k-ε model by means of a wind tunnel test and large-eddy simulation of the turbulence structure around a cube. *Journal of Wind Engineering and Industrial Aerodynamics* 35, 87-100.

Nakamura, Y. and Ozono, S. (1987). The effects of turbulence on a separated and reattaching flow. *Journal of Fluid Mechanics*, 178, 477-490.

Noda, H. and Nakayama, A. (2003). Free-stream turbulence effects on the instantaneous pressure and forces on cylinders of rectangular cross section. *Experiments in Fluids* 34, 332-344.

Pocha, J. J. (1971). *On unsteady flow past cylinders of square cross section*. Ph.D. Dissertation, Queen Mary University of London, United Kingdom.

Song, C. C. S., and Yuan, M. (1988). A weakly compressible flow model and rapid convergence method. *Journal of Fluids Engineering* 110, 441-455.

Vickery, B. J. (1966). Fluctuating lift and drag on a long cylinder of square cross-section in a smooth and in a turbulent stream. *Journal of Fluid Mechanics* 25, 481-494.